Acta Mechanica Sinica (2012) 28(5):1356–1366
DOI 10.1007/s10409-012-0142-3

RESEARCH PAPER

Experimental study on mechanical properties of methane-hydrate-bearing sediments

Xu-Hui Zhang · Xiao-Bing Lu · Li-Min Zhang · Shu-Yun Wang · Qing-Ping Li

Received: 26 October 2011 / Revised: 18 April 2012 / Accepted: 16 May 2012

Abstract Mechanical properties of methane hydrate-bearing-sediments (MHBS) are basic parameters for safety analysis of hydrate exploration and exploitation. Young's modulus, cohesion, and internal friction angle of hydrate-bearing sediments synthesized in laboratory, are investigated using tri-axial tests. Stress–strain curves and strength parameters are obtained and discussed for different compositions and different hydrate saturation, followed by empirical expressions related to the cohesion, internal friction angle, and modulus of MHBS. Almost all tested MHBS samples exhibit plastic failure. With the increase of total saturation of ice and methane hydrate (MH), the specimens' internal friction angle decreases while the cohesion increases.

Keywords Gas hydrate sediment · Tri-axial test · Cohesion · Internal friction angle · Elastic modulus

1 Introduction

Natural gas hydrate is a crystalline solid composed typically of methane gas and water molecules that is stable at high pressure and low temperature conditions. In the nature, gas hydrate is distributed extensively in ocean sediments, permafrost and deep lakes [1–4].

In recent years, methane hydrate has attracted great interest in scientific communities for the following reasons [5–20]:

(1) It is conservatively estimated that more than 50% of the 18.8 terratonnes of organic carbon present on the earth is in the form of gas hydrate, found either in marine sediments or in permafrost. Extraction of methane from hydrates could provide a future energy resource [6].

(2) Methane is a greenhouse gas 20 times potent than carbon dioxide [7]. The volume of methane currently bound in hydrate is thought to be many thousand times that held in the atmosphere. Either the changes in temperature or pressure can cause the instability of methane hydrate-bearing-sediments (MHBS). Loss of stability in seafloor hydrate could lead to sea-level rising and global climate change [8–10].

(3) Evidence suggests that dissociation of methane hydrate (MH) can be a trigger for long run-out submarine landslides [11–16]. It is reported that the reason of the biggest Storegga slide was hydrate dissociation induced by the increase of seawater temperature [14]. These huge events are known to have led in the past to major tsunamis and widespread flooding and devastation along continental littoral [15].

(4) Oil and gas exploration are now extending far off the continental shelf where hydrates can be present in relatively shallow layer below the sea bed. There is a concern that hydrocarbon exploration and development activities may trigger hydrate dissociation which may result in seabed slope instability [17–19]. Recently, the deepwater horizon explosion in gulf may be caused by dissociation of MH since the drilling rig had reached the sediments where the pressure and temperature is proper for hydrate formation [20, 21].

A common concern with submarine MH is to identify its global and local occurrence, concentration and form, and

The project was supported by the National Natural Science Foundation of China (11102209 and 11072245), the National High Technology Research and Development Program of China (863) and the Key Program of Chinese Academy of Sciences (KJCX2-YW-L02).

X.-H. Zhang (✉) · X.-B. Lu · S.-Y. Wang
Laboratory for Hydrodynamics and Ocean Enginnering, Institute of Mechanics, Chinese Academy of Sciences, 100190 Beijing, China
e-mail: zhangxuhui@imech.ac.cn
L.-M. Zhang
Department of Civil and Environmental Engineering, Hong Kong, University of Science and Technology, Hong Kong, China
Q.-P. Li
Research Centre, China Ocean Oil Co., 100027 Beijing, China

the most suitable methods for exploitation. Because MH exists only under very restricted conditions, it is difficult to determine their presence and properties by drilling or to bring undisturbed specimens to the laboratory for testing [22]. Another method of locating and characterizing hydrates comes from marine seismic geophysical records. However, the development, validation, and optimization of seismic surveying techniques requires an understanding of the relationship between sediment type, hydrate form, content, and physical and mechanical properties of the sediment [23, 24]. Properties of the porous host sediment affect the morphology and extent of hydrate growth, which in turn may alter the host sediment properties [25, 26].

The difficulty of drilling, sampling and synthesizing sediment containing MH is responsible for a lack of related mechanical properties [25]. Winters et al. [27] studied the mechanical properties of MHBS. The test results showed that both the strength and the compressive wave speed of MHBS are greater than that for sediments without methane hydrate (MH). The increment depends on the saturation and distribution of MH, and the properties of sediments.

Hyodo [28] investigated the relationship between mechanical properties and temperature, pore pressure, confining pressure and MH saturation. Experiments of Masui et al. [29, 30] showed that the strength of in-situ samples is the same as that of synthetic samples, although the stress-strain curves are different. The differences come mainly from the differences in initial void ratio and grain sizes. These results indicated that synthetic samples can be used to model in-situ MHBS.

Wei et al. [31] tested deformation and failure properties of carbon dioxide hydrate in sands, and the results showed that shear modulus and strength increased with carbon dioxide hydrate saturation. Yun et al. [32] used the tetrahydrofuran hydrate bearing sediments to conduct series tests, with hydrate saturation, confining pressure, and particle size of soil taken into account. Miyazaki et al. [33] studied artificial methane hydrate bearing sediments using drained tri-axial tests and found that the strength and stiffness increased with hydrate saturation and effective confining pressure.

At present, the mechanical data of hydrate-bearing sediments are lack quantitatively and the mechanical properties are expressed qualitatively. In this paper, tri-axial tests are carried out at low temperature (below freezing temperature) and high pressure conditions to study mechanical properties (e.g., elastic modulus and strength) of MHBS with various MH saturations. For comparison, the mechanical parameters of frozen ice-bearing sediments and water saturated sand are also obtained by tri-axial tests. Empirical formulas for strength parameters of MHBS are presented to explore the relationship between contents and strength parameters of hydrate, ice and soil skeleton.

2 Equipment and methods

2.1 Test apparatus

Tests were carried out in an apparatus developed at the Institute of Mechanics, Chinese Academy of Sciences (Fig. 1). The apparatus provides confining pressures ranging from 0 to 14 MPa with an accuracy of 0.5% (Fig. 2) and temperatures from –20°C to 20°C with an accuracy of 2.5% (Fig. 3). The maximum back-pressure provided by a gas-supply cylinder is 10 MPa. This allowed the necessary high pressure and low temperature conditions for achieving the formation of MH. A gas flow-meter was used to measure the total gas percolating into the specimen which is initially partially water saturated. Then hydrate is formed under proper pressure and temperature (Fig. 4 [34]).

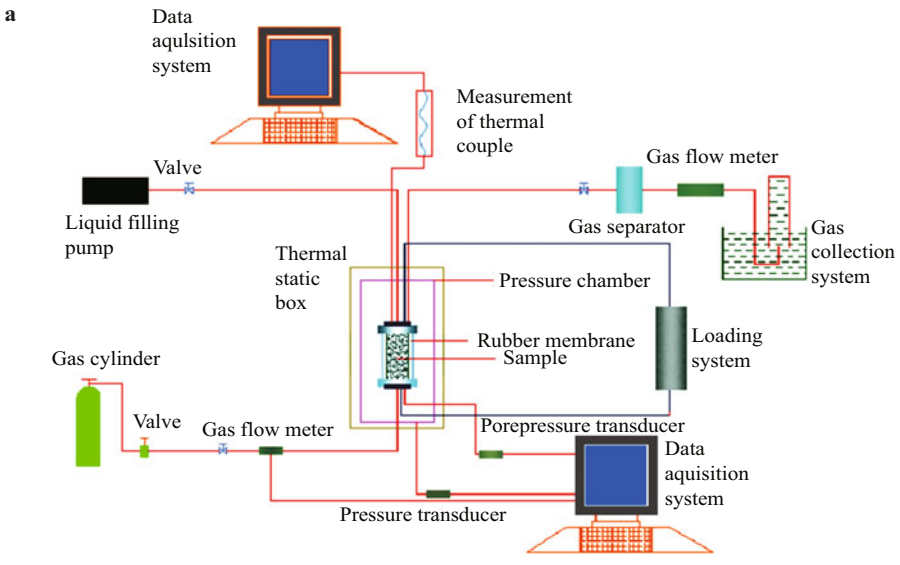

Fig. 1 Sketch of the apparatus for MHBS syntheses and tri-axial test. **a** The whole apparatus for MHBS syntheses and tri-axial test; **b** Integration of MHBS syntheses and tri-axial test

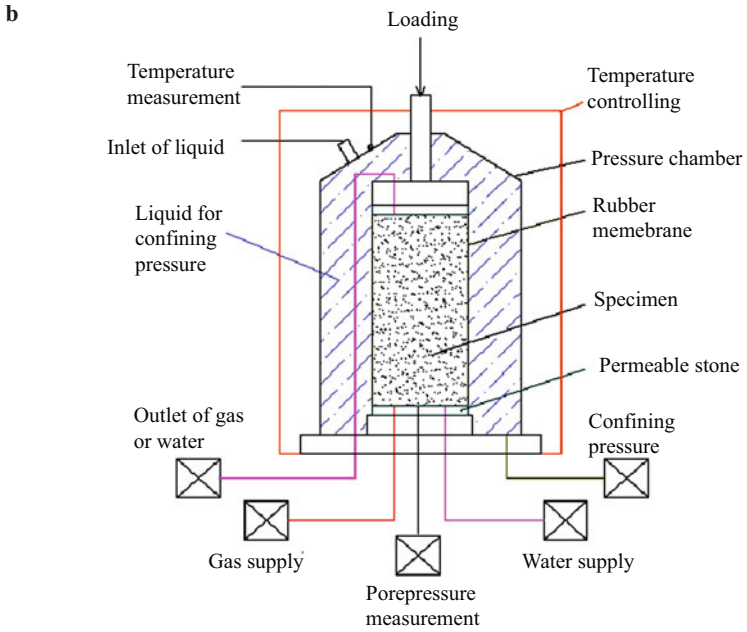

Fig. 1 Sketch of the apparatus for MHBS syntheses and tri-axial test. **a** The whole apparatus for MHBS syntheses and tri-axial test; **b** Integration of MHBS syntheses and tri-axial test (continued)

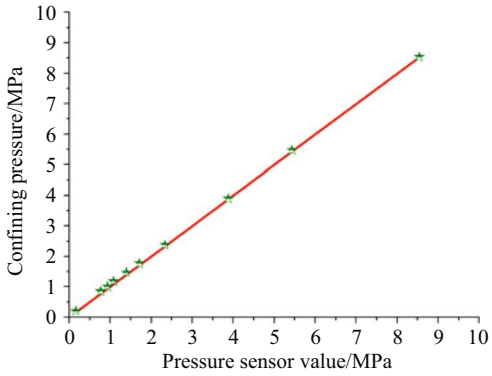

Fig. 2 Calibration of confining pressure

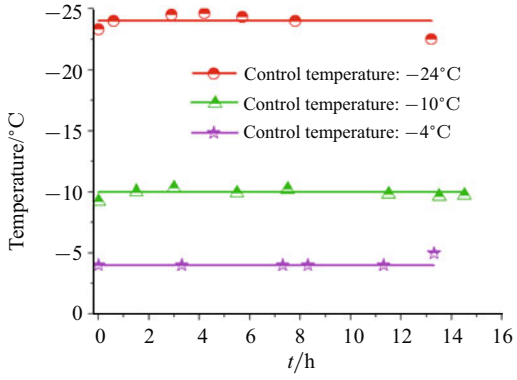

Fig. 3 Calibration of temperature control

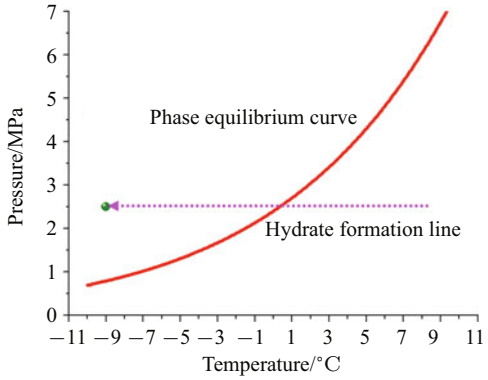

Fig. 4 Pressure and temperature condition for hydrate formation [46] (In our tests, 2.5 MPa and –9°C were chosen)

A gas collection system with a volume of 6 L was designed to measure the gas released from the specimen during dissociation (Fig. 5). In this system the water in two cylinders is pushed out once the methane gas is released from the specimen. The process can be described as follows: When methane gas is released from MHBS, the gas pressure is larger than the pressure in the collecting system which is equal to atmosphere pressure, so the water is pushed out until the pressures at two sides are equal. The gas volume is then obtained by measuring the displaced water with a precision of about 0.5%, because the gas volume under pressure of 0.1 MPa and temperature of 0°C is almost equal to the displaced water (the solubility of methane in water under this condition is ignorable).

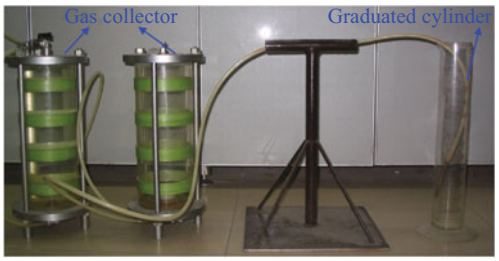

Fig. 5 Gas collection system

2.2 Test procedure

The material tested was a fine silty sand with dry density of 1.6 g/cm^3, maximum void ratio of 0.949 and minimum void ratio of 0.454. The grain size distribution is shown in Fig. 6.

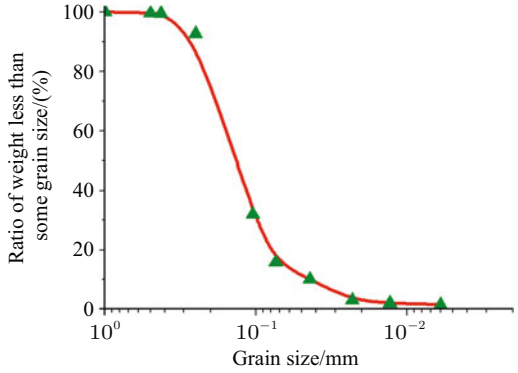

Fig. 6 Grain size distribution of fine silty sand (Grain size is expressed in terms of $\log_{10}$).

Phase equilibrium curves of MH in porous sediments are quite different from that of bulk MH. As the pore size decreases, higher pressure or lower temperature are needed for phase equilibrium compared with that of bulk hydrates. For an example, the super-cooling degree can be over −10°C as the pore size decreases to less than 10 nm. A radius of 60 nm is regarded as the critical value for the temperature offset in hydrate formation [35].

Three thin sections were cut from the top, middle, and bottom of a specimen by the sample cutting method in soil mechanics. Then the sections were covered with thin water layers on the surface and observed under a microscope with an accuracy of 2 μm to obtain pore-throat characteristics when the boundaries of pores and throats could be distinguished. Shown in Fig. 7 are the observed pore-throat structures. The channel between two neighboring white lines is called the pore throat; the area crossed by two or more throats is called the pore. For the specimen under test the mean radius of pore-throats is over 50 μm, thus the offset of temperature and pressure can be neglected.

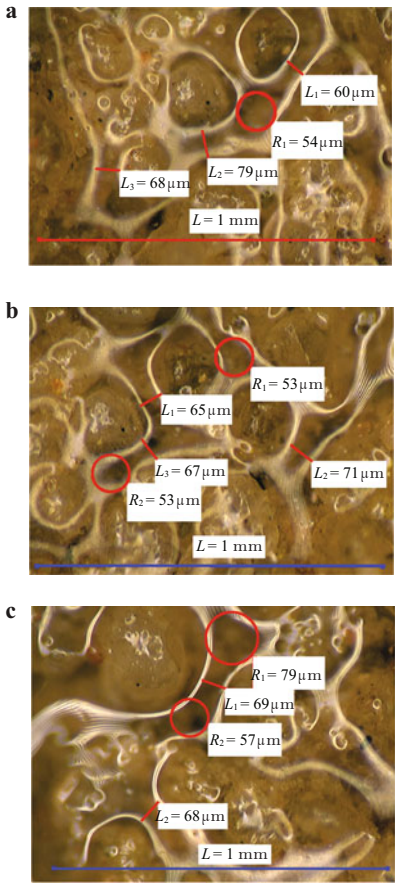

Fig. 7 The pore-throat structure of sand skeleton. **a** At the top; **b** At the middle; **c** At the bottom

In lack of microscopic observation technology, we took several specimens out of the cell after MH formation, checked whether the specimens were intact and hard. We found that the samples required great physical force to break the synthesized intactness.

The procedure can be described in five steps as follows:

(1) Prepared sand specimens (initially 10% water saturated in quality) with diameter and height of 39.1 mm and 80 mm, respectively, in a copper mold. Each specimen was sealed within a butyl rubber membrane (0.1 mm in thickness) to prevent subsequent methane gas migration.

(2) Placed the specimen into the tri-axial cell and pushed water into the specimen until a desired saturation was reached. A thermo-couple was attached to the cell wall to measure the temperature. The cell top was then fitted and a confining pressure was slowly applied. As this methane gas was pressurized into the specimen, the flow rate was controlled by a gas flow-meter. The rubber membrane was expanded to allow a peripheral gas supply around the specimen at a proper pressure difference between confining pressure and gas pressure, which was favorable for more uniform MH specimen. Then a pore pressure of 2.5 MPa was maintained 24 hours to induce methane gas dissolution in the pore water.

(This step was not necessary for preparing frozen specimens without MH.)

(3) The specimen temperature was gradually lowered to –9°C into the hydrate-stability range to form MH. When the gas flow into the specimen became insignificant and the pore pressure was stable after MH was formed, the temperature was increased to a value slightly above the hydrate-stability range for at least three hours to trigger MH dissociation. Temperature was decreased again to form MH. This process was repeated at least twice to increase the saturation of MH (It is called temperature oscillation method [36]).

(4) After the specimen were prepared, the excess gas was drained. An axial load was applied to the top of the specimen by a ram at a constant rate of 0.9 mm/min until the strain reached 15% during which the tests were un-drained. The axial displacement, axial force and pore pressure of the specimen were measured and recorded (here for un-drained condition, the volume strain could be neglected).

(5) The temperature was increased to dissociate the MH in the specimen. The volume of methane released during dissociation was measured by the collection system described in Sect. 2.1.

3 Test results and analysis

Hydrate saturation greatly affects the mechanical properties of MHBS. The initial water saturation of the specimen was controlled by the volume of water, V_w, percolated into the specimen before the formation of hydrate. The volume of methane gas, V_g, consumed during the formation of gas hydrate was obtained using the collecting system shown in Fig. 5. The hydrate saturation S_H and the ice saturation S_I can be calculated from Eqs. (1)–(3).

The hydrate saturation is obtained by the gas volume measured

$$S_H = \frac{V_H}{V_p} = \frac{\alpha V_g}{V_p}. \tag{1}$$

The ice saturation is equal to the difference between the total water content and that contained in the hydrate

$$S_I = \frac{V_I}{V_p} = \frac{\beta V_w}{V_p}, \tag{2}$$

where $\alpha = p_0 M_h/(RT_0\rho_h)$, $\beta = 1 - N_h M_w p_0 V_g/(\rho_w R T_0 V_w)$, V_p is the pore volume of the sediments, p_0 is 0.1 MPa, T_0 is 273.15 K, R is gas constant with a value of 8.31 J/(mol · K), M_h and M_w are molar mass of hydrate and water respectively, ρ_h and ρ_w are density of hydrate and water respectively, N_h is hydrate number (the number of water molecules corresponding to one methane molecule).

In this paper MH was formed at temperatures below 0°C, thus the pores were filled by ice except for MH. The Mohr–Coulomb type criterion is adopted here to describe the strength of MHBS [37]

$$\tau = \sigma \tan[\theta(\varepsilon_H, \varepsilon_I, \varepsilon_r)] + C(\varepsilon_H, \varepsilon_I, \varepsilon_r). \tag{3}$$

Here τ is the yield stress, σ is the normal stress, θ is the internal friction angle, C is the cohesion, ε_H is the volume percentage of hydrate, ε_I is the volume percentage of ice, ε_r is the volume percentage of soil skeleton. ε_H, ε_I, and ε_r are defined as function of porosity ϕ, S_H and S_I

$$\text{Volume percentage of MH: } \varepsilon_H = \phi S_H, \tag{4}$$

$$\text{Volume percentage of ice: } \varepsilon_I = \phi S_I, \tag{5}$$

$$\text{Volume percentage of soil skeleton: } \varepsilon_r = 1 - \phi. \tag{6}$$

We note that: (1) The specimen temperature was set at –9°C because MH specimens were synthesized relatively easily and the experimental results could be properly analyzed by solid mechanics; (2) When the total water saturation was above 90%, the sample would collapse or become curved during water saturating or MH formation due to partial soil softening; (3) The total saturation was set at about 80%, the respective saturation of ice and methane hydrate was changed above 10%, and then the change of mechanical parameters can be observed and analyzed clearly.

3.1 Test results for water-saturated sand

To obtain mechanical properties of non hydrate-bearing sand specimens, three water saturated sand specimens (named A1, B1 and C1) were prepared and tested in consolidated drained conditions under confining pressures of 2.5 MPa, 5 MPa and 10 MPa, respectively.

Figure 8a shows the stress-strain curves of the saturated sand. It is shown that the failure modes are all plastic (the stress increases linearly with the strain initially, and keeps constant until the engineering failure strain of 15% is achieved). The deviatoric stress ($\sigma_1 - \sigma_3$, σ_1 is the axial stress, σ_3 is the confining stress.) reaches about 20 MPa under a confining pressure of 10 MPa. Figure 8b shows that the effective cohesion and internal friction angle of the sand skeleton are 0.1 MPa and 30.5°, respectively.

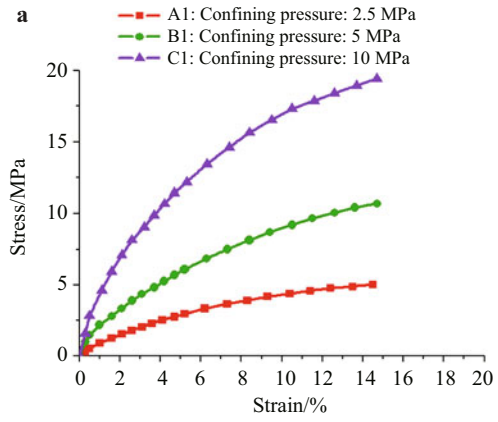

Fig. 8 Stress–strain curves and Mohr circles of water-saturated sediments. **a** Stress–strain curve; **b** Mohr circle

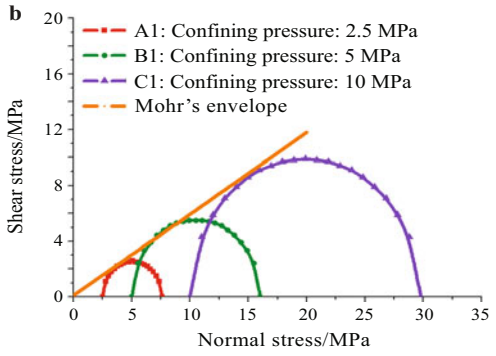

Fig. 8 Stress–strain curves and Mohr circles of water-saturated sediments. **a** stress–strain curve; **b** Mohr circle (contiuned)

3.2 Test results for frozen sediment

Three specimens of frozen sediment (named A2, B2 and C2) with ice saturations of 86.3%, 83.2% and 85.5% were prepared for triaxial tests under confining pressures of 2.5 MPa, 5.0 MPa and 10.0 MPa, respectively.

Failure modes of the three specimens are all plastic (Fig. 9a). The deviatoric stress reaches 10 MPa and 6 MPa under confined pressure of 10 MPa and 2.5 MPa, respectively. The drained conditions in tests of water saturated samples and the expansion in ice samples could lead to larger deviatoric stresses relative to that of frozen sediment. The cohesion and internal friction angle are 2.8 MPa and 9.6°, respectively (Fig. 9b). Compared with the water saturated sand, the cohesion increases significantly while the internal friction angle decreases significantly.

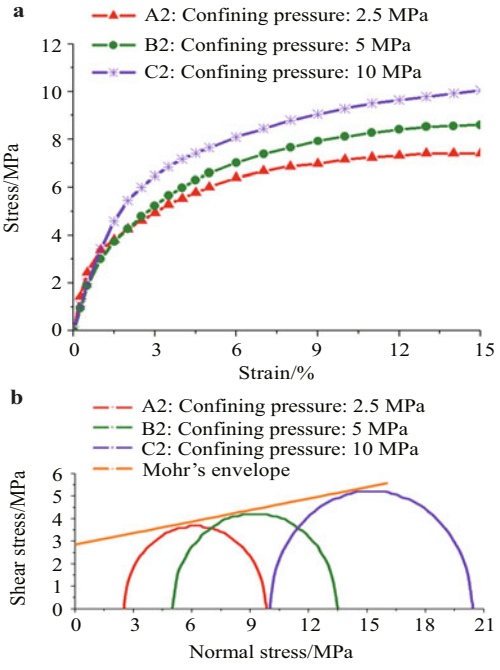

Fig. 9 Stress–strain curves and Mohr circles for the frozen sediment specimens. **a** Stress–strain curve; **b** Mohr circle

3.3 Test results for MHBS

In this section, three groups of tests (each group had three specimens) were carried out to analyze the effects of MH saturation under undrained conditions.

The three specimens in the first group (named A3, B3, and C3) were prepared with MH saturations of 29.6%, 31.1% and 31.1%, respectively, and ice saturations of 59.6%, 55.5% and 51.1%, respectively. Triaxial tests were carried out under confining pressures of 2.5 MPa, 5.0 MPa and 10.0 MPa, respectively. Because the pores were filled with ice and hydrate, there was no pore pressure in tests.

Figure 10a shows the stress-strain curves from the three tests. This group of specimens had low MH saturations and high ice saturations, which may be the reason that the failure modes are all plastic similar to those of the iced sediment shown in Fig. 6a. The deviatoric stresses are 6 MPa and 3 MPa under confined pressure of 10 MPa and 2.5 MPa, respectively. The results indicate that the strength of MHBS were lower than those of frozen sediments, which is in agreement with the results of Winters et al [27]. Figure 10b shows that the cohesion and internal friction angle of MHBS are 1.2 MPa and 8.5°, respectively. Note that the total saturations of ice and MH in the three specimens are 89.2%, 86.6% and 82.2%, respectively. It is clear that the cementation of ice with grains is greater than that of MH compared with the test results for frozen sediment. The internal friction of MHBS is affected weakly by the formation of either ice or MH in the pores.

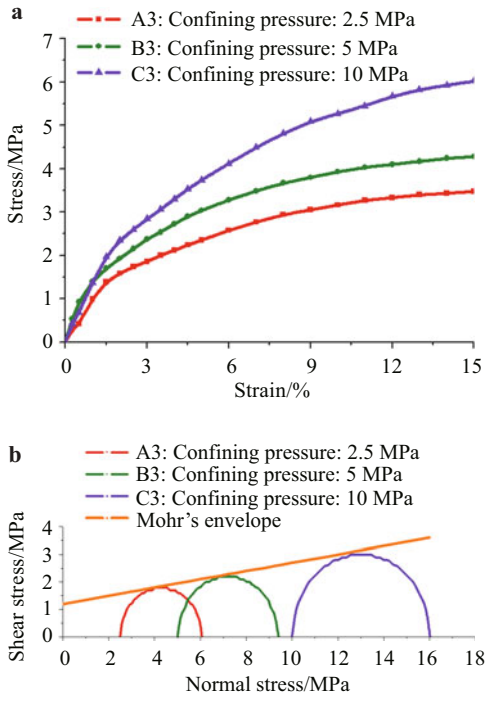

Fig. 10 Stress–strain curves and Mohr circles for MHBS (A3, B3, C3). **a** Stress–strain curve; **b** Mohr circle

The three specimens in the second group (named A4, B4, and C4) had MH saturations of 43%, 48.9% and 51.3% and ice saturations of 31.5%, 26.4% and 24.4%, respectively. The same confining pressures of 2.5 MPa (A4), 5 MPa (B4) and 10 MPa (C4) as those in the tests for the first group were used.

Figure 11a shows the stress-strain curves of the three specimens. It can be seen that B4 and C4 are still plastic failure. However, A4 presents a brittle failure (there is a peak stress). The cohesion and internal friction angle are 1.16 MPa and 12.4°, respectively (Fig. 11b). Although the cohesion is almost the same, the internal friction angle is greater than that of A3, B3 and C3.

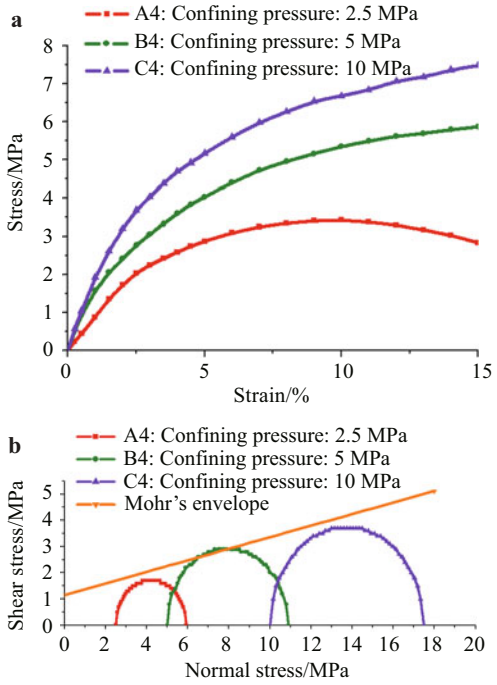

Fig. 11 Stress–strain curves and Mohr circles for MHBS (A4, B4, C4). **a** Stress–strain curve; **b** Mohr circle

The three specimens in the third group (named A5, B5 and C5) with MH saturations of 26.3%, 26.3% and 30%, respectively, and ice saturations of 45.8%, 45.8% and 42.6%, respectively, were also carried out under confining pressures of 2.5 MPa, 5 MPa and 10 MPa, respectively.

The measured stress-strain curves, as can be seen from Fig. 12a, are similar to that of A4, B4, and C4. However, this group of specimens has a smaller cohesion and a greater internal friction angle, which are 0.7 MPa and 19.3° (Fig. 12b), respectively, compared with those for the first and second groups.

Generally speaking, with the increase of total saturation of ice and MH, the specimens' internal friction angle decreases while the cohesion increases. Under the same saturation, the increase of ice content leads to the increase of cohesion.

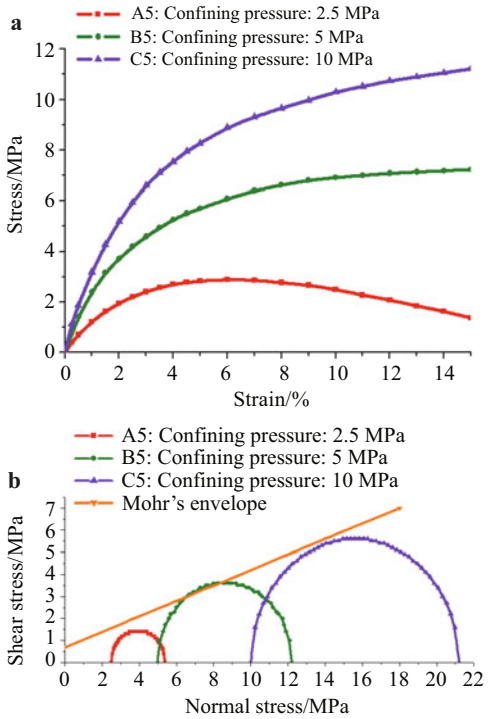

Fig. 12 Stress–strain curve and Mohr circle of MHBS (A5, B5, C5). **a** Stress–strain curve; **b** Mohr circle

It is believed that the cementation (The grains are cemented by ice and MH.) is enhanced with the increase of total saturation of ice and hydrate, which leads to strong cementing force among sand particles. The strength and modulus of sediments containing MH are influenced by a number of factors: strain rate, temperature, consolidation stress, grain size, density and even gas hydrate cage occupancy. The pores of MHBS are filled with MH, which increases the tendency for dilation during shear [28]. Although the water saturated sand used in tests is not cemented, cementation develops once it contains MH.

4 A model for the strength of MHBS

4.1 An empirical formula for strength parameters of MHBS under different conditions

It is well known that the formation of MH will change the properties of MHBS. Generally, ten parameters determine the mechanical properties: ε_H, ε_r, ε_I, C_H, C_r, C_I, T_e, P_e, $\dot{\varepsilon}$, θ_H, θ_r and θ_I, in which C_H, C_r, C_I are cohesions of hydrate, soil skeleton, and ice, respectively, T_e, P_e are phase equilibrium temperature and pressure of hydrate formation, $\dot{\varepsilon}$ is shear rate, θ_H, θ_r, θ_I are friction angles of hydrate, soil skeleton, and ice. Hyodo [28] showed that the temperature and pressure during the formation of gas hydrate sediments (GHS) had no effects on the strength. The strain rate (strain in unit time) in tests is generally small. So assuming that T_e, P_e, $\dot{\varepsilon}$ have little effect on MHBS's modulus, meanwhile the cohesion of matrix is $C_r = 0$, thus the cohesion and the internal friction angle of MHBS are functions of ε_H/C_H, ε_I/C_I

and $\varepsilon_H/\tan\theta_H$, $\varepsilon_I/\tan\theta_I$, $\varepsilon_r/\tan\theta_r$, respectively

$$\frac{1}{C} = f\left(\frac{\varepsilon_H}{C_H}, \frac{\varepsilon_I}{C_I}\right),$$
$$\frac{1}{\tan\theta} = g\left(\frac{\varepsilon_H}{\tan\theta_H}, \frac{\varepsilon_I}{\tan\theta_I}, \frac{\varepsilon_r}{\tan\theta_r}\right), \quad (7)$$

Let $\varepsilon_t = \varepsilon_H + \varepsilon_I$ and assume

$$\frac{\varepsilon_t}{C} = \frac{\varepsilon_H}{C_H} + \frac{\varepsilon_I}{C_I}, \quad (8)$$

and

$$\frac{\varepsilon_t}{\tan\theta} = \frac{\varepsilon_H}{\tan\theta_H} + \frac{\varepsilon_I}{\tan\theta_I} + \frac{\varepsilon_r}{\tan\theta_r}. \quad (9)$$

Here, the unknowns C_H, C_I, $\tan\theta_H$, $\tan\theta_I$ and $\tan\theta_r$ are expected to be obtained by fitting experimental data of ε_t, ε_H, ε_I, ε_r, C and $\tan\theta$.

Comparison of the test data for the cohesion and internal friction is presented in Table 1 and the data obtained from Eqs. (1) and (2) are shown in Tables 2 and 3. It is shown that the test data are in good agreement with the fitted values.

Table 1 C, ϕ of water-saturated, hydrate-bearing and frozen sediments

Specimen	Confining pressure in shearing tests/MPa	Hydrate saturation/(%)	Ice saturation/(%)	Total saturation/(%)	Internal friction angle/(°)	Cohesion/MPa
A1	2.5	0	0	0		
B1	5	0	0	0	37	0
C1	10	0	0	0		
A2	2.5	0	86.3	86.3		
B2	5	0	83.2	83.2	9.6	2.85
C2	10	0	85.5	85.5		
A3	2.5	29.6	59.6	89.2		
B3	5	31.1	55.5	86.6	8.5	1.2
C3	10	31.1	51.1	82.2		
A4	2.5	43	31.5	74.5		
B4	5	48.9	26.4	75.3	12.4	1.16
C4	10	51.3	24.4	74.7		
A5	2.5	26.3	45.8	72.1		
B5	5	26.3	45.8	72.1	19.3	0.7
C5	10	30	42.6	72.6		

Table 2 Comparison of cohesion between test and fitted data

Type of sediments	Fraction of hydrate ε_H	Fraction of ice ε_I	Total fraction of ice and hydrate $\varepsilon_t = \varepsilon_H + \varepsilon_I$	Experimental value C_T/MPa	Fitted value C/MPa	Error $\left\lvert\frac{C_T - C}{C_T}\right\rvert$
Group 2	0	0.34	0.34	2.85	2.01	29%
Group 3	0.12	0.22	0.34	1.2	1.16	3%
Group 4	0.19	0.11	0.30	1.16	0.88	24%
Group 5	0.11	0.18	0.29	0.8	1.12	40%
Group 6*	0.10	0	0.10	0.60	0.66	10%

* Hydrate sediments with skeleton of Toyoura sand

Table 3 Comparison of test and fitted data of internal friction angle

Type of sediments	Fraction of hydrate ε_H	Fraction of ice ε_I	Total fraction of ice and hydrate $\varepsilon_t = \varepsilon_H + \varepsilon_I$	Type of value sediments	Experimental θ_T/(°)	Fitted value θ/(°)	Error $\left\lvert\frac{\theta_T - \theta}{\theta_T}\right\rvert$
Group 1	0.60	0	0	0.60	33	37.9	14.8%
Group 2	0.60	0	0.34	0.94	9.6	9.57	0.3%
Group 3	0.60	0.12	0.22	0.94	8.5	10.8	27%
Group 4	0.60	0.19	0.11	0.90	12.4	12.8	3%
Group 5	0.60	0.11	0.18	0.89	19.3	11.8	38.8%

4.2 An empirical formula for elastic modulus of MHBS

A dimensionless expression is expressed as follows using the ten parameters ε_H, ε_r, ε_I, E_H, E_r, E_I which are important in determining the elastic modulus of MHBS

$$\frac{E_r}{E} = f\left(\frac{E_r}{E_H}, \frac{E_r}{E_I}, \frac{E_r}{\sigma_c}, \varepsilon_H, \varepsilon_r, \varepsilon_I\right). \tag{10}$$

Since ice, hydrate and the sand skeleton of MHBS are all solid phases, a linear expression of modulus related to the Reuss model and weighted average of the three-phase Wood equation [38, 39] is developed

$$\frac{\varepsilon_t}{E} = a\frac{\varepsilon_H}{E_H} + b\frac{\varepsilon_I}{E_I} + c\frac{\varepsilon_r}{E_r}, \tag{11}$$

in which a, b and c are three coefficients.

According to the test data shown in Table 4, E_H and E_I are valued as 8 200 MPa and 9 500 MPa, respectively [40], the coefficients a, b and c may be obtained by the least squares method: $a = 117.30$, $b = 34.55$, $c = 1.03$. The comparison of modulus by tests and theory are shown in Table 5. It is shown that they are quite close to each other.

Table 4 Summary of elastic modulus and yield stresses of hydrate and frozen sediments

Specimen	Hydrate saturation/(%)	Ice saturation/(%)	Total saturation/(%)	Elastic modules/MPa
A1	0	0	0	121.9
B1	0	0	0	378.9
C1	0	0	0	601.6
A2	0	86.3	86.3	566
B2	0	83.2	83.2	377
C2	0	85.5	85.5	415
A3	29.6	59.6	89.2	117
B3	31.1	55.5	86.6	212
C3	31.1	51.1	82.2	170
A4	43	31.5	74.5	94.3
B4	48.9	26.4	75.3	208
C4	51.3	24.4	74.7	226
A5	26.3	45.8	72.1	158
B5	26.3	45.8	72.1	287
C5	30	42.6	72.6	453

Table 5 Comparison between test and simulated elastic modulus

Label	Confining pressure σ_c/MPa	Fraction of skeleton ε_s	Fraction of hydrate ε_H	Fraction of ice ε_I	Total fraction ε_t	Experimental value E_T/MPa	Fitted value E/MPa	Error $\left\|\frac{E_T - E}{E_T}\right\|$
A1	2.5	0.60	0	0	0.60	122	118	3%
B1	5	0.60	0	0	0.60	379	368	3%
C1	10	0.60	0	0	0.60	602	584	3%
B2	5	0.60	0	0.333	0.933	377	328	13%
C2	10	0.60	0	0.342	0.942	415	415	0%
A3	2.5	0.60	0.118	0.238	0.956	117	126	8%
B3	5	0.60	0.124	0.222	0.946	212	223	5%
A4	2.5	0.60	0.172	0.126	0.898	94.3	112	18%
B4	5	0.60	0.196	0.106	0.902	208	186	11%
C4	10	0.60	0.205	0.098	0.903	226	207	8%
A5	2.5	0.60	0.105	0.183	0.888	158	122	22%
B5	5	0.60	0.105	0.183	0.888	287	232	19%

5 Conclusions

Consolidated undrained tri-axial tests on frozen, methane hydrate-bearing sediments and consolidated drained triaxial tests on water saturated sand were carried out in a special tri-axial apparatus at the Institute of Mechanics, Chinese Academy of Sciences. The confining pressures adopted were 2.5 MPa, 5 MPa and 10 MPa. It is shown that the formation of ice and MH significantly change the mechanic properties of MHBS. An empirical model for the strength of MHBS is presented.

Failure modes of samples are generally plastic (e.g. there is no peak stress). In tests presented in this paper, the maximum saturation of hydrate is less than 40%, thus the MHBS is still stress dependent [41]. With the increase of total saturation of ice and MH, the specimens' internal friction angle decreases a little while the cohesion increases. Under the same saturation, the increase of ice content leads to an increase of cohesion.

The modulus and internal friction angle and cohesion of MHBS can be expressed as a linear combination of each component's saturation and corresponding parameters (e.g., modulus, friction and cohesion) based on mixed theory.

The results in this paper are expected to serve as a reference for estimating Yang's modulus and strengths of MHBS from the contents of hydrate, ice and skeleton. In the future, more widely varied saturations, the homogeneity of hydrate distribution in sediments and the effects of compositions and microstructures of soil skeleton will be considered. Further, the formulation of plastic deformation of hydrate-bearing sediments referred to the model by Aryanpour and Farzaneh [42] will be explored also which can provide a basis for evaluating the possible geo-hazards in hydrate exploitation.

References

1 Sloan, Jr. E. D.: Clathrate Hydrates of Natural Gases. Marcel Dekker Inc., New York (1998)

2 Kvenvolden, K. A.: Methane hydrate-A major reservoir of carbon in the shallow geosphere. Chem. Geol. **71**, 41–45 (1988)

3 Kvenvolden, K. A., Lorenson T. D.: The global occurrence of natural gas hydrate. Geophysical Monograph **124**, 3–18 (2001)

4 Koh, C. A.: Towards a fundamental understanding of natural gas hydrates. Chem. Soc. Rev. **31**, 157–167 (2002)

5 Clayton, C. R. I., Priest, J. A., Best, A. I.: The effects of disseminated methane hydrate on the dynamic stiffness and damping of a sand. Geotechnique **55**, 423-434 (2005)

6 Kvenvolden, K. A., Lorenson, T. D.: The global occurrence of natural gas hydrate. Geophysical Monograph **124**, 3–18 (2001)

7 Shine, K. P., Derwent, R. G., Wuebbles, D. J., et al.: Radiative forcing of climate. In: Climate Change, The IPCC Scientific Assessment, edited by Houghton, J. T., Jenkins, G. J., Ephraums, J. J., Cambridge University Press, New York, 41–68 (1990)

8 Xu, W., Germanovich, L. N.: Excess pore pressure resulting from methane hydrate dissociation in marine sediments: A theoretical approach. J. Geophys. Res. **111**, B01104 (2006)

9 Sultan, N.: Comment on "Excess pore pressure resulting from methane hydrate dissociation in marine sediments: A theoretical approach" by Wenyue Xu and Leonid N. Germanovich. J. Geophys. Res. Solid Earth **112**, 78–84 (2007)

10 McIver, Richard, D.: Role of naturally occurring gas hydrate in sediment transport. American Association of Petroleum Geologists, Bulletin **66**, 789–792 (1982)

11 Bugge, T., Befring, S., Belderson, R. H., et al.: A giant three-stage submarine slide off Norway. Geo-Marine Letters **7**, 191–198 (1987)

12 Driscoll, N. W., Weissel, J. K., Goff, J. A.: Potential for large scale submarine slope failure and tsunami generation along the US mid-Atlantic coast. Geology **28**, 407–410 (2000)

13 Bouriak, S., Vanmste, M., Saoutkine, A.: Inferred gas hydrates and clay diapers near the Storegga slide on the southern edge of the Vφring Plateau, off shore Norway. Marine Geology **163** 125–148 (2000)

14 Jung, W. Y., Peter, R. V.: Effects of bottom water warming and sea level rise on holocene hydrate dissociation and mass wasting along the Norwegian–Barents Continental Margin. Journal of Geophysical Research **109**, B06104 (2004)

15 Kayen, R. E., Lee, H. J.: Pleistocene slope instability of gas hydrate-laden sediment on the Beaufort Sea margin. Mar. Geotechnol. **10**, 125–141 (1991)

16 Milkov, A. V.: World distribution of submarine mud volcanoes and associated gas hydrate. Marine Geol. **167**, 29–42 (2000)

17 Briaud, J. L., Chaouch, A.: Hydrate melting in soil around hot conductor. J. Geotech. Geoenvir. Eng. **123**, 645–653 (1997)

18 Chaouch, A., Briaud, J. L.: Post melting behavior of gas hydrates in soft Ocean sediments. OTC8298 1–11 (1997)

19 Zhang, X. H., Lu, X. B., Li, Q. P., et al.: Thermally induced evolution of phase transformations in gas hydrate sediment. SCIENCE CHINA-Physics, Mechanics & Astronomy **53**, 1530–1535 (2010)

20 Brooks, J. M., Cox, B. H., Bryant, W. R., et al.: Association of gas hydrates and oil seepage in the gulf of Mexico. Organic Geochemistry **10**, 221–234 (1986)

21 Kwon, T. H., Cho, G. C., Santamarina, J. C.: Gas hydrate dissociation in sediments: pressure temperature evolution. Geochemistry Geophysics Geosystems **9**, Q03019 (2008)

22 Francisca, F., Yun, T. S., Ruppel, C., et al.: Geophysical and geotechnical properties of near sea-floor sediments in the northern gulf of Mexico gas hydrate province. Earth and Planetary Science Letters **237**, 924–939 (2005)

23 Wu, B. H., Zhang, G. X., Zhu, Y. H.: Progress of gas hydrate investigation in China offshore. Earth Science Frontiers **10**, 177–189 (2003)

24 Guerin, G., Goldberg, D., Meltser, A.: Characterization of in situ elastic properties of gas hydrate-bearing sediments on the Blake Ridge. Journal of Geophysical Research **104**, 17781–17795 (1999)

25 Lee, M. W., Collett, T. S.: Elastic properties of gas hydrate-bearing sediments. Geophysics **66**, 763–771 (2001)

26 Winters, W. J., Waite, W. F., Mason, D. H., et al.: Methane gas hydrate effect on sediment acoustic and strength properties. Journal of Petroleum Science and Engineering **56**, 127–135 (2007)

27 Winters, W. J., Pecher, I. A., Waite, W. F., et al.: Physical properties and rock physics models of sediment containing natural

and laboratory-formed methane gas hydrate. American Mineralogist **89**, 1221–1227 (2004)
28 Hyodo, M., Nakata, Y., Yoshimoto, N., et al.: Shear behavior of methane hydrate-bearing sand. In: Proc. 17th Int. Offshore and Polar Eng. Conf., Lisbon, Portugal, 1326–1333 (2007)
29 Masui, A., Haneda, H., Ogata, Y. et al.: Mechanical properties of sandy sediment containing marine gas hydrates in deep sea offshore Japan. In: Proc. 17th Int. Offshore and Polar Eng. Conf., Ocean Mining Symposium, Lisbon, Portugal, 53–56 (2007)
30 Masui, A., Haneda, H., Ogata, Y., et al.: Effect of methane hydrate formation on shear strength of synthetic methane hydrate sediment. In: Proc. 15th Int. Offshore and Polar Eng. Conf., Seoul, Korea, 364–369 (2005)
31 Wei, H. Z., Yan, R. T., Chen, P., et al.: Deformation and failure behavior of carbon dioxide hydrate-bearing sands with different hydrate contents under tri-axial shear tests. Rock and Soil Mechanics **32**(Supp.2), 198–203 (2011)
32 Yun, T. S., Santamarina, J. C., Rupple, C.: Mechanical properties of sand, silt and clay containing tetrahydrofuran hydrate. Journal of Geophysical Research **112**, B04106 (2007)
33 Miyazaki, K., Masui, A., Sakamoto, Y., et al.: Triaxial compressive properties of artificial methane-hydrate-bearing-sediment. Journal of Geophysical Research **116**, B06102, (2011)
34 Llamedo, M., Anderson, R., Tohidi, B.: Thermodynamic prediction of clathrate hydrate dissociation conditions in mesoporous media. American Mineralogist **89**, 1264–1270 (2004)
35 Turner, D., Sloan, E. D.: Hydrate phase equilibrium measurements and predictions in sediments. In: Proceedings of the Fourth International Conference on Gas Hydrates, Yokohama, Japan, 327–330 (2002)
36 Huang, D. Z., Fan, S. S.: The promotion of methane hydrate formation in quiescent system. Chemistry **5**, 379–384 (2005)
37 Freij-Ayoub, R., Tan, C., Clennel, B., et al.: A well-bore stability model for hydrate bearing sediment. J. Petro. Science Engrg. **57**, 209–220 (2007)
38 Helgerud, M. B., Dvorkin, J., Nur, A.: Rock physics characterization for gas hydrate reservoirs: elastic properties. Annals of the New York Academy of Sciences **9**, 49–58 (2000)
39 Lee, M. W., Collett, T. S.: Elastic properties of gas hydrate-bearing sediments. Geophysics **66**, 763–771 (2001)
40 Cox, J.: Natural Gas Hydrates: Properties, Occurrence and Recovery. Butterworth, Woburn, USA (1983)
41 Waite, W. F., Santamarina, J. C., Cortes, D. D., et al.: Physical properties of hydrate-bearing sediments. Reviews of Geophysics **47**, 1–38 (2009)
42 Aryanpour, G., Farzaneh, M.: Analysis of axial strain in one-dimensional loading by different models. Acta Mech. Sin. **26**, 745–753 (2010)